C. R. Mecanique 346 (2018) 890–902

Contents lists available at ScienceDirect

Comptes Rendus Mecanique

www.sciencedirect.com

Jet noise modelling and control / Modélisation et contrôle du bruit de jet

Wavepacket models for subsonic twin jets using 3D parabolized stability equations

Daniel Rodríguez [a,*], Mamta R. Jotkar [b,1], Elmer M. Gennaro [c],

[a] Laboratory of Theoretical and Applied Mechanics (LMTA), Graduate Program in Mechanical Engineering (PGMEC), Department of Mechanical Engineering, Universidade Federal Fluminense, Niterói, RJ 24210-240, Brazil
[b] Centro Tecnológico, Universidade Federal do Rio de Janeiro, Rio de Janeiro, RJ 21941-914, Brazil
[c] São Paulo State University (UNESP), Campus São João da Boa Vista, SP 13874-149, Brazil

ARTICLE INFO

Article history:
Received 14 June 2017
Accepted 3 January 2018
Available online 19 July 2018

Keywords:
Twin jets
Flow instability
Parabolized Stability Equations
Wavepackets
Turbulence modelling

ABSTRACT

An extension of the classical parabolized stability equations to flows strongly dependent on the two cross-stream spatial directions and weakly dependent on the streamwise one is applied to model the large-scale structures present in twin-jet configurations. The existence of these unsteady flow structures, usually referred to as wavepackets, has been demonstrated in the literature for both subsonic and supersonic round jets, along with their relation to the generation of highly directional noise emitted in the aft direction. The present study considers twin-jet configurations with different separations at high Reynolds number and subsonic conditions. The existing instability modes for the twin-jet mean flow, their dependence on the separation of the two jets, and the interaction between the wavepackets originating from the two jets is investigated here. Arising from the axisymmetric mode for single round jets, two dominant modes are found for twin jets: a varicose one, relatively insensitive to jets' proximity, but likely to be efficient in radiating noise; a sinuous one, whose amplification is strongly dependent on the jets' distance, and which can be expected to produce weaker acoustic signatures.

1. Introduction

Jet noise reduction is a technological problem that has received continuous effort since the appearance of commercial jet airliners in the early 1950s. Modern commercial aircrafts feature very high-bypass-ratio turbofans that are considerably quieter than the early-day jet engines. However, mission requirements and architecture of tactical fighters impose high exhaust speed and limited nozzle cross-section area, demanding alternative noise reduction strategies. In addition to a deep understanding of the underlying physics, the development of noise reduction mechanisms requires efficient and reliable models for noise prediction that could be used in the design and optimization cycle of passive devices, or as reduced-order models for active control devices. With a view of achieving this objective, simple models that relate the properties of the turbulent jet mean flow with the noise radiated to the far-field are sought for here.

* Corresponding author.
E-mail addresses: danielrodriguez@id.uff.br, danielrodalv84@gmail.com (D. Rodríguez), mmtjotkar@gmail.com (M.R. Jotkar), elmer.gennaro@unesp.br (E.M. Gennaro).
[1] Present address: Nonlinear physical chemistry unit, Université Libre de Bruxelles, Belgium.

https://doi.org/10.1016/j.crme.2018.07.002
1631-0721/

Following the seminal works of Mollo–Christensen [1], the relation between the dominant components of the far-field noise radiated by high-speed jets and large-scale fluctuations in the turbulent mixing region, coherent over several nozzle diameters, has been the subject of growing research [2]. Evidence amassed in the last decades show that, indeed, radiated sound is highly directional for both subsonic and ideally-expanded supersonic jets [3–5]. While temporal intermittency is a characteristic of both far- and near-field pressure fluctuations, the radiated sound is found to be highly correlated with large-scale, low-frequency fluctuations in the mixing region, and with the very few azimuthal modes, for single isolated jets [6–8]. The existence of coherent structures in turbulent jets was first identified by Crow and Champagne [9], and their resemblance to instability waves for harmonically-forced supersonic jets suggested the use of linear instability analysis for modeling them [10,11]. The presence of wavepackets in subsonic natural high-speed jets was finally demonstrated over the last decade [12–14], as well as the ability of linear stability calculations to model them faithfully. In particular, parabolized stability equations (PSE) were demonstrated to deliver a notable agreement with simulation and experimental near-fields for both subsonic and supersonic jets, at a very low computational cost [15,16,13,14,17,18]. Alternative methodologies, based on the comparatively more expensive two-dimensional eigenmode problems, have been used to compute global wavepackets in the time and frequency domains [19–21]. More recently, one-way linearized equations have been proposed as an improved method for modeling the wavepacket using a parabolic integration, which overcomes some of the limitations known for PSE [22].

With few exceptions, most of the tactical fighters developed since the 1960s feature fuselage-embedded twin-jet engines. Additionally, multi-tube nozzles have been investigated as possible jet noise suppressors. Experiments on these configurations showed that twin-jet configurations can result in a reduction of the far-field noise with respect to the equivalent isolated jet [23,24]. By varying the spacing between the nozzles, two different mechanisms leading to noise suppression were identified. The first one is related to the interaction between the turbulent mixing region of each jet, which can modify and reduce the sound sources, and only occurs for closely-spaced nozzles. The second one is due to the acoustic shielding that one jet exerts on the sound emitted from the other one. Although noise reduction occurs at all jet spacings, it is only important in the plane defined by the jet centers.

This paper is concerned with the modeling of the coherent structures present in twin-jet configurations as instability wavepackets. As opposed to single round jets, instability analyses for twin jets are scarce in the literature, which is partially explained by the mathematical complexity of the latter. The mean turbulent flow corresponding to isolated round jets is axisymmetric, which enables the introduction of azimuthal Fourier modes and requires spatial discretization on the radial direction alone. Bipolar coordinates were used by Morris [25] and Green and Crighton [26] to study the inviscid instability of two axially-homogeneous parallel jets. They identified the counterparts of the different azimuthal Fourier modes known for single jets and classified them according to the symmetries about the jet-center plane and the plane normal to it. Jet interactions were found to be important only when the distance between jets was below ~ 3 times the nozzle diameter.

An extension of the standard parabolized stability equations is used in this paper for modeling the wavepackets in subsonic turbulent twin jets. First introduced by Blackburn and Sherwin [27], the three-dimensional parabolized stability equations (3D PSE) are applicable to mean flows with a strong variation of its properties on the cross-stream plane and a mild downstream variation. Separation of scales for the time-periodic disturbances results in a downstream-marching problem analogous to the standard PSE, but allowing disturbances of arbitrary shape along the cross-stream plane. An *ad hoc* locally-parallel stability problem is derived based on the 3D PSE operators to provide the adequate near-nozzle initial conditions. The computed solutions implicitly account for the interaction of the wavepackets on each jet, including the possible mutual stabilization or destabilization. The methodology is applied to a tailored mean flow, constructed by superposition of the axial velocity fields measured experimentally for a single round jet with Mach number $M_j = 0.4$ and Reynolds number $Re = 4.2 \times 10^5$, based on jet exit velocity and nozzle diameter [14,28]. The analyses performed herein are focused on the frequency range in which the highly-directional turbulent-mixing noise was found to be dominant in subsonic single round jets. In terms of the Strouhal number $St = fD/U_j$ defined by the frequency f and the jet exhaust velocity U_j and diameter D, the frequency range is $St = [0.25 - 0.65]$. Additionally, linear stability computations aiming to model the wavepackets recovered maximum amplifications and amplitudes for this range, both for subsonic and supersonic regimes (e.g., [12,13,19,14,2,20,21]).

The rest of the paper is organized as follows. Sections 2.1 and 2.2 introduce the 3D PSE approach and the spatial locally-parallel stability eigenvalue problem associated with it, while 2.3 briefly presents the numerical techniques used. The construction of the mean flows is discussed in section 3.1. Results from the locally-parallel stability at the near-nozzle section and the 3D PSE computations are respectively presented in sections 3.2 and 3.3. Finally, some discussion of the results and conclusions close the paper.

2. Methodology

The total turbulent flow field is separated into a mean (i.e. time-averaged) flow and temporal fluctuations $\mathbf{q}(\mathbf{x}, t) = \bar{\mathbf{q}}(x) + \mathbf{q}'(\mathbf{x}, t)$, where $\mathbf{x} = (x, y, z)^\intercal$ is the vector or coordinates in a Cartesian system, t is the time and $\mathbf{q} = (u, v, w, \rho, p, T)^\intercal$ is a vector containing all the fluid variables of interest: the velocity components u, v, w in the x, y, z directions respectively, density ρ, pressure p and temperature T. Physical quantities are made dimensionless using the jet diameter D, and the free-stream sound speed c_∞ and density ρ_∞. Pressure is scaled with $\rho_\infty c_\infty^2$ and temperature with $(\gamma - 1)T_\infty$, where γ is the ratio of specific heats. The jet Mach number is defined as $M_j = U_j/c_\infty$, with U_j being the exit velocity. The statistical

stationarity of the turbulent flow allows for the introduction of Fourier modes for frequency $\omega = 2\pi M_j St$ (St being the Strouhal number), as

$$\mathbf{q}'(\mathbf{x}, t) = \sum_{\omega} \breve{\mathbf{q}}_{\omega}(\mathbf{x}) \mathrm{e}^{-\mathrm{i}\omega t} + c.c. \tag{1}$$

where $c.c.$ stands for the complex conjugate.

2.1. Three-dimensional parabolized stability equations

Based on the multiple-scale approach and originally devised for the study of Tollmien–Schlichting waves on transitional boundary layers, PSE accounts for a slow divergence of the mean flow properties and has been shown to deliver results comparable to those of direct numerical simulations for convectively unstable laminar and transitional flows [29,30]. More recently, PSE has been extensively used as a model for the spatial evolution of large-scale coherent wavepackets present in single round turbulent jets, commonly known as wavepackets [15,16,13,14,17,18], and a good agreement has been found with coherent structures educed either from experiments or large eddy simulations, at least up to the end of the potential core.

The fluctuations $\breve{\mathbf{q}}_{\omega}(\mathbf{x})$ are decomposed into a shape function $\tilde{\mathbf{q}}_{\omega}$, which is also slowly varying along the streamwise direction x, and a rapidly varying wave-like part:

$$\breve{\mathbf{q}}_{\omega} = A_{\omega}(x)\, \tilde{\mathbf{q}}_{\omega}(x, y, z) = A_{\omega}(x_0) \exp\left(\mathrm{i} \int_{x_0}^{x} \alpha_{\omega}(\xi)\, \mathrm{d}\xi \right) \tilde{\mathbf{q}}_{\omega}(x, y, z) \tag{2}$$

The complex quantity $\alpha_{\omega} = \alpha_r + \mathrm{i}\alpha_i$ is a streamwise wavenumber, for which a slow variation with x is assumed as well. The streamwise coordinate x_0 is the location where the PSE integration is initialized, typically a cross-section close to the nozzle lip for jets. Upon introduction of (2) into the linearized compressible Navier–Stokes, continuity and energy equations, and neglecting terms involving second-order derivatives of the fluctuations on x, one arrives at the system of equations

$$\mathbf{L} \frac{\partial \tilde{\mathbf{q}}_{\omega}}{\partial x} = \mathbf{R} \tilde{\mathbf{q}}_{\omega} \tag{3}$$

where the linear operators $\mathbf{L}$ and $\mathbf{R}$ depend on the mean flow quantities and their first and second spatial derivatives, wavenumber α, frequency ω, physical parameters Re, M_j, Pr, γ, and spatial differentiation operators on the cross-stream directions: $\mathcal{D}_y, \mathcal{D}_z, \mathcal{D}_{yy}, \mathcal{D}_{yz}$ and $\mathcal{D}_{zz}$.

The decomposition (2) and the governing equations (3) do not define uniquely the solution, as the spatial wave growth can be absorbed into the shape function or the complex amplitude. Following Herbert [31], the following normalization condition is imposed in order to eliminate the exponential dependence from $\tilde{\mathbf{q}}_{\omega}$:

$$\iint_{\Omega} \mathbf{q}_{\omega}^{*} \frac{\partial \tilde{\mathbf{q}}_{\omega}}{\partial x}\, \mathrm{d}y\, \mathrm{d}z = 0 \tag{4}$$

where * denotes complex conjugation and Ω is the cross-stream domain.

The parabolized stability equations (3) constitute a downstream-marching problem along the slow coordinate x. Consequently, it requires inlet conditions for the shape functions $\tilde{\mathbf{q}}_{\omega}$ and wavenumber α_{ω} at some location x_0. Common practice is to derive a locally-parallel linear stability analysis, consistent with the PSE matrices, and employ its results in the determination of the inlet conditions. When high-fidelity experimental or numerical simulation data is available, this approach provides a theoretically-founded technique for the determination of representative amplitudes and phases [17,28].

2.2. Locally-parallel linear stability analysis

The matrix operators involved in the PSE approximation are used here to derive a locally-parallel stability eigenvalue problem (EVP), which is obtained by assuming $\mathrm{d}\alpha/\mathrm{d}x \approx 0$ and $\partial \breve{\mathbf{q}}_{\omega}/\partial x \approx \mathrm{i}\alpha \breve{\mathbf{q}}_{\omega}$ [17]. From this approximation, one arrives at the following EVP:

$$\mathrm{i}\,\alpha\, \mathbf{L} \hat{\mathbf{q}}_{\omega} = \mathbf{R}\, \hat{\mathbf{q}}_{\omega} \tag{5}$$

Operators $\mathbf{R}$ and $\mathbf{L}$ are the same as in (3), but particularized for $\alpha = \mathrm{d}\alpha/\mathrm{d}x = 0$. For a given cross-stream plane x and real frequency ω, the solution to (5) delivers a set of complex eigenvalues α_n and their corresponding eigenfunctions $\hat{\mathbf{q}}_n(y, z)$. For unbounded mean flows like the present ones, classical theory [32,33] shows the existence of a fixed number of continuous branches, related to the uniform flow surrounding the jets, in addition to an indefinite number of discrete eigenmodes associated with localized mean flow shear. The numerical solution to (5), based on the spatial discretization of the linear operators (described in the next subsection) results into a discretized representation of the continuous branches.

2.3. Numerical methods

The numerical resolution of both the PSE (3) and local stability EVP (5) requires the spatial discretization of the two-dimensional linear operators $\mathbf{R}$ and $\mathbf{L}$ in the cross-stream yz planes. It is well known that the computational cost associated with the memory storage and the operational time of these multi-dimensional operators become prohibitive if standard methods for one-dimensional problems are used [34,35]. Based on our own previous experiences [36], we developed a new stability code that combines variable-stencil high-order finite differences and sparse algebra, exploiting the banded structure of the differentiation matrices. In this work, a 7-point stencil is used, which results in the optimal balance between convergence of results and computational cost [37].

A rectangular domain is considered for the cross-stream planes $\Omega = [-y_\infty, y_\infty] \times [-z_\infty, z_\infty]$. A coordinate transformation is used to concentrate points for the two spatial directions in the central region of the computational domain, where the jets are located:

$$\eta = \eta_\infty \frac{\sinh\left(a(\xi - 1/2)\right)}{\sinh\left(a/2\right)} \tag{6}$$

where η is the mapped coordinate in the physical domain (e.g., y or z), ξ is the coordinate in the computational domain ($\xi = [0, 1]$), η_∞ is the maximum (positive and negative) value of η, and a is a real number that controls the clustering of points. The value $a = 2.5$ is used in the present calculations.

The Cartesian coordinate system allows for the use of standard finite differences for the independent differentiation on y and z, resulting in the differentiation matrices $\mathcal{D}_y$ and $\mathcal{D}_z$ for first-order derivatives and $\mathcal{D}_{yy}$ and $\mathcal{D}_{zz}$ for second-order derivatives. The same stencil is used for first- and second-order differentiation matrices, which allows for the control of the matrix structure, required for the efficiency of the sparse implementation. The cross-differentiation matrix is then obtained as $\mathcal{D}_{yz} = \mathcal{D}_y \times \mathcal{D}_z$.

After discretization of the linear operators, the EVP (5) is solved using a sparse in-house implementation of the shift-and-invert Arnoldi algorithm [38,39]. First, the EVP is formally transformed into

$$(\mathbf{R} - \mathrm{i}\,\sigma\,\mathbf{L})^{-1}\mathbf{L}\,\hat{\mathbf{q}} = \mu\,\hat{\mathbf{q}} \tag{7}$$

where $\mu = -\mathrm{i}\,(\alpha - \sigma)^{-1}$ and the subscript ω drop for simplicity of notation. The shift parameter σ is used to control the center of the eigenvalue window, such that the eigenvalues closer to σ are the first to converge. Arnoldi's algorithm requires the resolution of a number of linear problems, which is accomplished using the MUMPS package [40].

The spatial discretization of the linear operators describing the PSE (3) is identical to the one for the EVP. Parabolized stability equations are a spatial-marching problem that is integrated along the streamwise direction using an implicit Euler scheme. This solution technique is known to present convergence problems due to the residual ellipticity of PSE, associated with the upstream-propagating wave solutions in the operators [41]. In practice, this limits the minimum step size that can be used to obtain stable solutions. Andersson et al. [42] proposed a stabilization procedure that enables the use of smaller step sizes, by means of adding a term proportional to the truncation error of the implicit scheme:

$$\mathbf{L}\,\frac{\partial \tilde{\mathbf{q}}_\omega}{\partial x} = \mathbf{R}\,\tilde{\mathbf{q}}_\omega + s\,\mathbf{R}\,\frac{\partial \tilde{\mathbf{q}}_\omega}{\partial x} \tag{8}$$

where s is a positive real number. The minimum step size for a stable integration can be estimated as

$$\Delta x_{\min} \geq \left(\alpha_r + \frac{\omega M_j^2}{1 - M_j^2}\right)^{-1} - 2\,s \tag{9}$$

The fixed values $\Delta x = 0.25$ and $s = 0.1$, determined for the stable integration of the lowest frequency considered, are used for all the calculations presented here. Increasing the value of s up to $s = 1$ did not produce noticeable differences in the computed wavepacket evolution.

Matrix equation (8) is recast in the form of (3) by introducing the operator $\tilde{\mathbf{L}} = \mathbf{L} - s\,\mathbf{R}$.

The solution $\tilde{\mathbf{q}}_{i+1}$ at the axial step x_{i+1} is obtained from the knowledge of the solution at a previous station $\tilde{\mathbf{q}}_i$ by solving the linear system

$$\tilde{\mathbf{L}}_{i+1}\left(\frac{\tilde{\mathbf{q}}_{i+1} - \tilde{\mathbf{q}}_i}{\Delta x}\right) = \mathbf{R}_{i+1}\tilde{\mathbf{q}}_{i+1} \tag{10}$$

where $\Delta x = x_{i+1} - x_i$. Since operators $\mathbf{R}$ and $\tilde{\mathbf{L}}$ depend on the mean flow quantities, they also depend on the streamwise station. The linear systems (10) are also solved using MUMPS. In order to adjust the value of α_{i+1} so that the normalization condition (4) is satisfied, the solution to the linear system is iterated together with

$$\alpha_{i+1}^{(k+1)} = \alpha_{i+1}^{(k)} - \frac{\mathrm{i}}{\Delta x}\frac{\iint_\Omega \tilde{\mathbf{q}}_{i+1}^{*}(\tilde{\mathbf{q}}_{i+1} - \tilde{\mathbf{q}}_i)\,\mathrm{d}y\,\mathrm{d}z}{\iint_\Omega \tilde{\mathbf{q}}_{i+1}^{*}\tilde{\mathbf{q}}_{i+1}\,\mathrm{d}y\,\mathrm{d}z} \tag{11}$$

where k is the iteration index, until α is converged up to a tolerance of 10^{-5}.

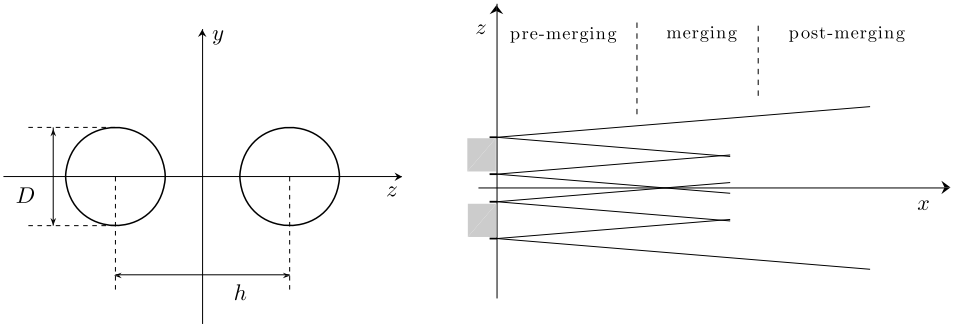

Fig. 1. Twin-jet mean flow configuration and geometry: (left) Nozzle-lip cross-stream plane $y-z$; (right) transversal plane $x-z$ showing the streamwise evolution of the jet shear layers.

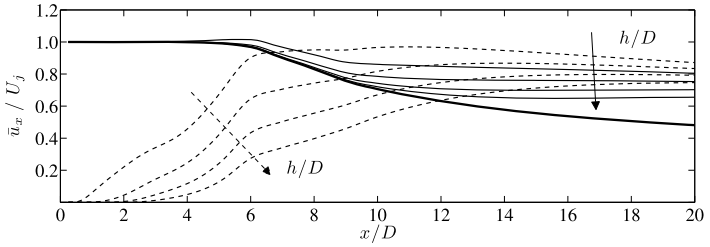

Fig. 2. Axial velocity for the twin-jet flow, as a function of the streamwise coordinate. The solid lines correspond to the coordinates of a nozzle $(y,z) = (0,h/2)$, and the dashed lines to the symmetry plane $(y,z) = (0,0)$. The different curves correspond to $h/D = 1.25, 1.5, 1.75$ and 2, increasing in the direction of the arrows. The thick solid line is the centerline velocity for one isolated jet.

3. Results

3.1. Tailored twin-jet base flow construction

A tailored mean flow field is considered for twin-jet configurations, constructed by combining the flow fields corresponding to isolated round jets. The analytical expression used by Troutt & MacLaughlin [43] and Tam & Burton [44] describes the single-jet axial velocity profile as a function of three parameters: the axial velocity u_c, the annual-mixing layer thickness δ, and the transversal extent of the potential core R. For a spatially-developing jet, these three quantities are functions of the axial coordinate x:

$$\frac{\bar{u}_x}{U_j} = \begin{cases} u_c(x), & r < R(x) \\ u_c(x)\exp\left[-(r-R(x)^2)/\delta^2(x)\right], & r \geq R(x) \end{cases} \tag{12}$$

In previous works [14,28], hot-wire anemometry data was used to determine $u_c(x), \delta(x)$, and $R(x)$ for an isolated round jet at different exhaust Mach numbers, following a procedure similar to that of Gudmundsson & Colonius [13]. A trip wire was used to ensure that the boundary layer internal to the nozzle was turbulent, and the Reynolds number based on the exhaust velocity U_j and nozzle diameter D was $Re = 4.2 \times 10^5$. The functions fitted for the mean jet flow corresponding to $M_j = 0.4$ are used in the present work.

Mean flows corresponding to a twin-jet configuration are obtained by considering two jets of the form (12), aligned with the x-direction and with centers placed symmetrically on the coordinates $(y,z) = (0,-h/2)$ and $(y,z) = (0,h/2)$. The nozzle lips lay on the $x = 0$ plane. Fig. 1 gives a schematic representation of the problem, where the geometry may be defined entirely using the distance between the nozzle centers h. The total axial velocity is obtained as the sum of the two jets, which is a rigorous model close to the nozzle lips, in the pre-merging region. Once the shear layers of the two jets meet, it is expected that non-linear interactions, present in the real flow, produce a mean flow that deviates to some extent from the model. However, the qualitative features of the mean flow remain consistent with experimental observations [45]. Fig. 2 shows the downstream evolution of the axial velocity at the nozzle center and in the mid-point between the jets. The velocity rise in the mid-plane is associated with the merging of the jets. The pre-merging region extends for distances comparable to the jet potential core when $h/D \geq 1.25$, and the effects of potential core closure and jet merging will appear simultaneously. While the two effects could be isolated by increasing the separation between jets or artificially reducing the divergence rates of the individual jets, realistic configurations present potential core closure and jet merging, and such isolation is not done here.

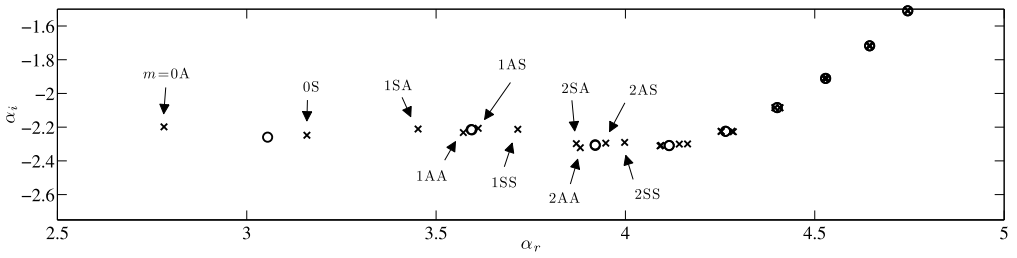

Fig. 3. Locally-parallel stability eigenspectra, for single-jet (circles) and twin-jet configuration with $h = 1.5\,D$ (crosses). $St = 0.5$ and $x = 0.25\,D$.

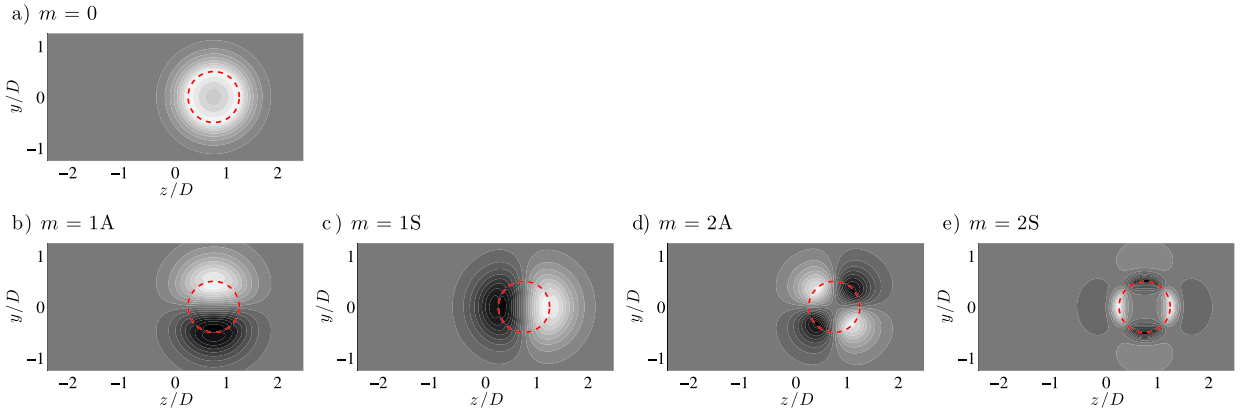

Fig. 4. Pressure eigenfunctions corresponding to Kelvin–Helmholtz modes $m = 0$, $m = 1$ and $m = 2$ for a single jet. $St = 0.5$, $x = 0.25\,D$.

A zero mean pressure gradient is assumed, and the Crocco–Busemann relation particularized for the isothermal jet

$$\frac{\bar{T}}{T_\infty} = \left(M_j - \frac{\bar{u}_x}{c_\infty}\right)\frac{\bar{u}_x}{2c_\infty} + \frac{1}{\gamma - 1} \tag{13}$$

is used to determine the mean temperature $\bar{T}$. The density $\bar{\rho}$ field is obtained from the state equation. The cross-stream mean velocity is neglected.

3.2. Locally-parallel stability results

The locally-parallel stability analysis used here considers disturbances with arbitrary shape in the cross-stream section. When applied to a single round jet, it must recover the same results as those obtained by more classical approaches used for axisymmetric flow (e.g., [46,28]). In particular, eigenmodes of the form $\exp(im\theta)$, where θ is the azimuthal angle with respect to axis z and $m = 0, \pm1, \pm2, \pm3\ldots$ is the corresponding wavenumber, are to be recovered by the analysis in a natural manner. Fig. 3 (circles) shows a representative eigenspectrum, corresponding to a single jet with center located at $(y, z) = (0, 0.75\,D)$, cross-stream plane $x = 0.25\,D$ and $St = 0.5$. Although the computational domain $\Omega = [-7, 7] \times [-7, 7]$ is used for the spatial resolution $N_y \times N_z = 601 \times 601$, convergence of the leading discrete Kelvin–Helmholtz eigenvalues is achieved, up to the third representative digit, with the smaller domain $\Omega = [-5, 5] \times [-3, 3]$ and resolution $N_y \times N_z = 501 \times 301$. The pressure components of the eigenfunctions corresponding to Kelvin–Helmholtz instability modes $m = 0$, $m = 1$ and $m = 2$ are shown in Fig. 4. The contours in this figure, as well as in subsequent Figs. 5 and 7–10, are evenly spaced between $\pm$ the maximum absolute value of the field quantity represented, white and black representing maxima positive and negative values, respectively. The background gray color corresponds to the zero level. Instabilities with $|m| \geq 1$ are represented by two eigenmodes in the analysis, with the same eigenvalue and identical spatial structure except for a rotation on the $y - z$ plane, so any azimuthal rotation of the spatial structure is captured by the linear combination of the two eigenmodes.

Fig. 3 also shows the analogous eigenspectrum for a twin-jet configuration, with jet centers located at $(y, z) = (0, \pm 0.75D)$ (jet separation $h = 1.5\,D$). The crosses denote the corresponding eigenvalues. Careful inspection of the eigenfunctions (Fig. 5) relates the eigenmodes to those of the single-jet configuration. The presence of the second jet doubles the number of eigenmodes corresponding to each Kelvin–Helmholtz mode, so that two eigenmodes exist for $m = 0$ and four for each of the $|m| \geq 1$ modes. The second jet also breaks the azimuthal-rotation symmetry of the eigenfunctions, and distinct eigenvalues are obtained for the equivalents of the m modes. A new classification for each m-mode is introduced on account of their symmetric or antisymmetric behavior with respect to the y and z axes. Figs. 5(a–b) show the pressure

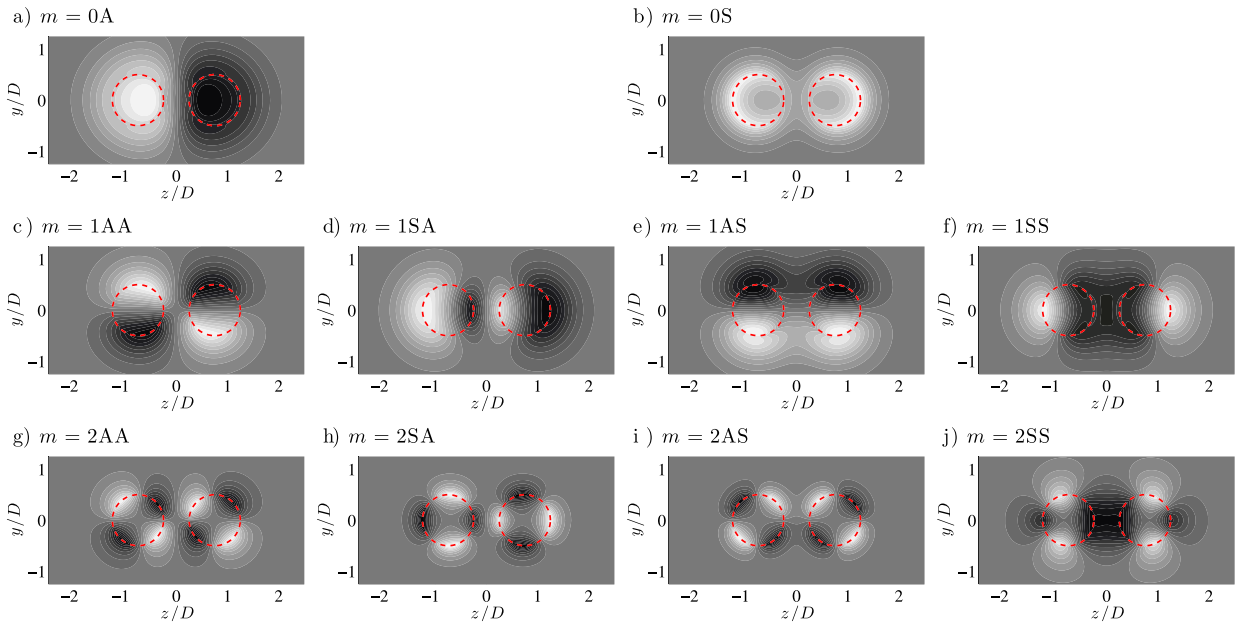

Fig. 5. Pressure eigenfunctions corresponding to Kelvin–Helmholtz modes $m = 0$, $m = 1$ and $m = 2$ for twin jets separated by $h/D = 1.5$. $St = 0.5$, $x = 0.25\,D$.

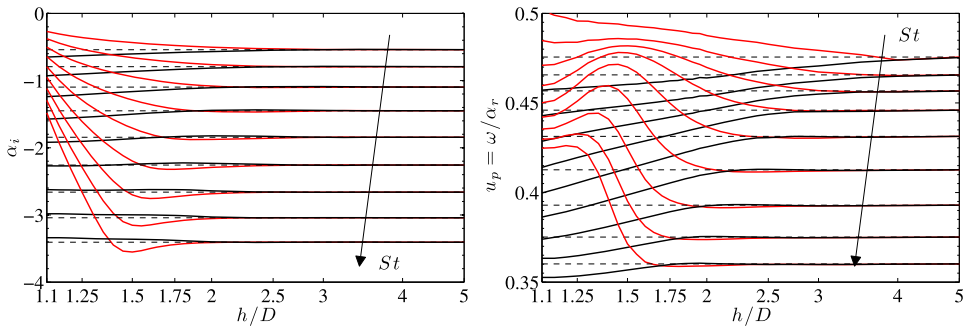

Fig. 6. Spatial growth rate α_i (left) and phase velocity $c_p = \omega/\alpha_r$ (right) corresponding to the $m = 0$ S (black lines) and $m = 0$ A (red lines) Kelvin–Helmholtz eigenmodes, as a function of the jet separation h, from the locally-parallel analysis at $x = 0.25\,D$. The Strouhal numbers are $St = 0.25, 0.3, 0.35, 0.4, 0.45, 0.5, 0.55, 0.6$ and 0.65, increasing in the direction of the arrow.

components of modes $m = 0$ S and $m = 0$ A, symmetric and antisymmetric over $y = 0$, respectively. Figs. 5(c–j) show modes AA, SA, AS and SS for $m = 1$ and $m = 2$, where the first letter denotes symmetry (S) or antisymmetry (A) on the $y = 0$ axis, and the second one on the $z = 0$ axis. This terminology is more complete than defining these modes as sinuous or varicose, as different modes of each kind are present, and more descriptive than that used by Morris [25]. Fig. 3 also shows that the influence of the jet proximity on the eigenmodes is inversely proportional to the azimuthal wavenumber m: the two eigenvalues corresponding to $m = 0$ for the twin-jet flow are different, and also differ from the single-jet ones. The twin-jet eigenmodes gradually converge towards the isolated jet ones as m is increased. This behavior is explained by the asymptotic decay of the single-jet eigenfunctions, the rate of which is proportional to $\sim r^{-1/2}\exp(-r\sqrt{\alpha^2 - \omega^2})$. For a fixed frequency ω, the axial wavenumber α increases with increasing m, resulting in a slower phase speed and a faster radial decay of the fluctuations.

The literature provides evidence that, for single subsonic round jets, wavepackets with $m = 0$ are correlated with the highly-directional far-field noise [5,2,14]. This is due to (i) the longer characteristic size of the wavepackets in the axial direction, as compared to helical modes, which is related to the instability properties of axisymmetric waves, (ii) the slower radial decay of $m = 0$ Bessel functions that represent acoustic radiation, and (iii) the absence of the partial noise cancellation associated with $+m$ and $-m$ Fourier modes when $|m| \geq 1$. Consequently, when considering twin jets, it can be expected that the wavepackets more relevant to noise generation are those corresponding to $m = 0$. Visualization of the asymptotic behavior of the cross-plane pressure field for large r shows that $m = 0$ S (Fig. 5.b) results into axisymmetric (i.e. $m = 0$) pressure fluctuations of varicose nature, while $m = 0$ A (Fig. 5.a) behaves like a $m = 1$, sinuous mode.

Fig. 6 shows the dependence of the spatial growth rate $-\alpha_i$ and phase velocity $c_p = \omega/\alpha_r$ with the jet separation for Strouhal numbers between 0.25 and 0.65. The results show that the jet interactions are stronger for lower frequencies. This

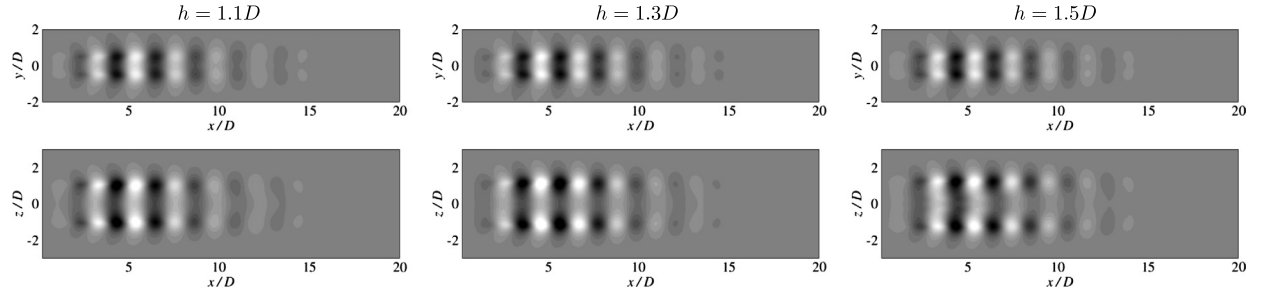

Fig. 7. Pressure field on the $z = 0.5h$ plane (top row) and $y = 0$ plane (bottom row), for mode $m = 0$ S, for three jet spacing $h/D = 1.1, 1.3$ and 1.5 and $St = 0.3$.

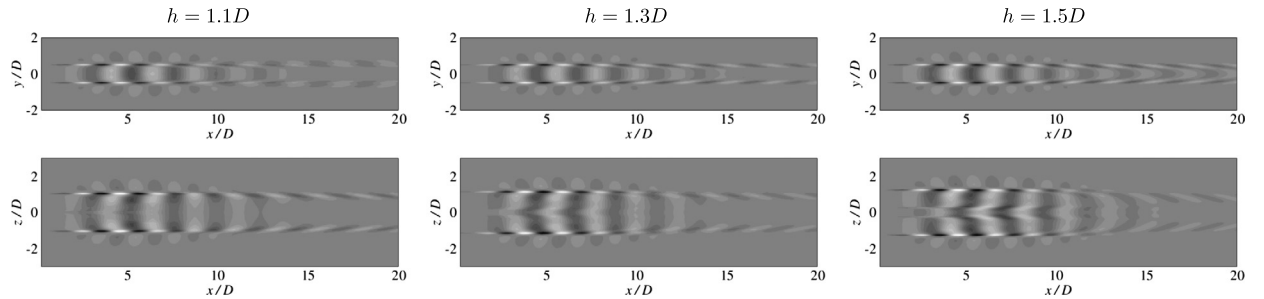

Fig. 8. Axial velocity field on the $z = 0.5h$ plane (top row) and $y = 0$ plane (bottom row), for mode $m = 0$ S, for three jet spacing $h/D = 1.1, 1.3$, and 1.5, and $St = 0.3$.

is explained by the asymptotic radial decay of the eigenfunctions, which recovers Bessel functions. Higher frequencies (and azimuthal wavenumbers) correspond to faster radial decays, and consequently the two jets need to be closer to experience comparable effects. Jet proximity decelerates the symmetric mode, while having a mild effect on its instability. For $St \leq 0.5$, $m = 0$ S is slightly destabilized, and stabilized for higher frequencies. The effect on the asymmetric mode is found to be stronger: destabilization occurs for a bounded range of jet separations, which depends strongly on St. As the frequency is increased, the peak growth rate increases, but the range of jet separations for instability and the most amplified frequency are reduced. Phase velocities of the $m = 0$ A mode exhibit non-monotonous variations with h and St, but in general they are increased with respect to their isolated-jet counterparts. Present results agree qualitatively with inviscid analyses of supersonic jets of finite-width mixing layer [25].

3.3. Three-dimensional parabolized stability equations

Once provided with a turbulent mean flow $\tilde{\mathbf{q}}$ (discussed in section 3.1) and an initial condition, obtained from the resolution of an *ad hoc* locally-parallel stability problem (section 3.2), the 3D PSE can be integrated to compute the spatially-evolving instability waves that model the statistical wavepackets.

In the following, computations initialized with $m = 0$ S and $m = 0$ A Kelvin–Helmholtz modes are considered. As discussed in the previous section, these eigenmodes can be expected to be most relevant for noise radiation. Figs. 7 and 8 show the pressure and axial velocity fields corresponding to 3D PSE computations initiated with the $m = 0$ S mode, for $St = 0.3$ and jet spacing $h/D = 1.1, 1.3$ and 1.5. The planes shown are the one containing the jet centers ($y = 0$) and the vertical one corresponding to one jet center ($z = 0.5h$). Figs. 9 and 10 show the analogous fluctuating flow fields for computations initialized with the $m = 0$ A mode.

The pressure fields corresponding to $m = 0$ S show an initial amplitude growth that extends for the first 5–6 diameters from the nozzle followed by a decay, resembling results for single jets [13,28]. Pressure and velocity fluctuations are found to be stronger in the external part of the twin-jet system than in the merging region between the two jets. Velocity fluctuations show the same qualitative behavior as for single jets, attaining peak values at approximately the same axial locations.

While the effects of jet proximity are found to be limited to mild quantitative differences on the wavepackets computed for $m = 0$ S modes, clear qualitative differences are observed in the pressure and velocity fields corresponding to $m = 0$ A modes (Figs. 9–10). As suggested by locally-parallel analyses in the vicinity of the nozzle (Fig. 6), jet proximity stabilizes these wavepackets, which is evident in the pressure fields and especially in the $x - z$ plane. As opposed to $m = 0$ S modes, velocity and pressure fluctuations are stronger in the merging region between the jet cores. For $m = 0$ A modes, velocity fluctuations in the vertical planes $z = 0.5h$ attain peak values at approximately the same axial locations. Conversely, when the transversal plane $y = 0$ is monitored, velocity fluctuations are found to achieve their maxima downstream of the pressure peak and extend farther with a milder decay rate. This different behavior may be attributed to the merging of the two

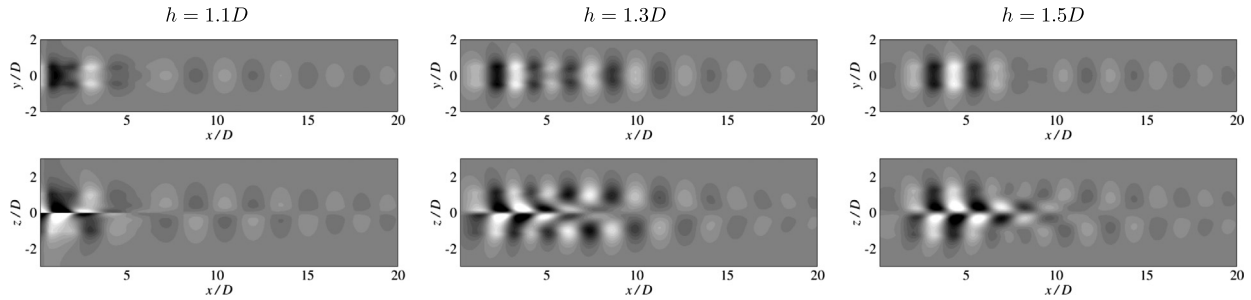

Fig. 9. Pressure field on the $z = 0.5h$ plane (top row) and $y = 0$ plane (bottom row), for mode $m = 0$ A, for three jet spacing $h/D = 1.1, 1.3$, and 1.5, and $St = 0.3$.

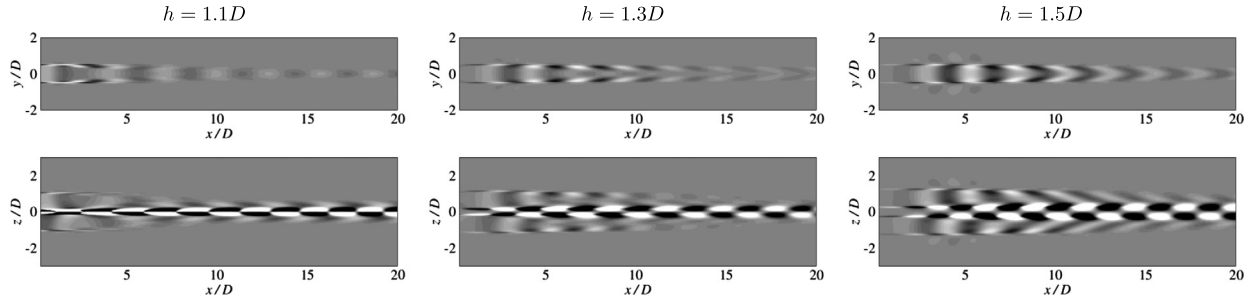

Fig. 10. Axial velocity field on the $z = 0.5h$ plane (top row) and $y = 0$ plane (bottom row), for mode $m = 0$ A, for three jet spacing $h/D = 1.1, 1.3$, and 1.5, and $St = 0.3$.

jets. The appearance of strong fluctuations of hydrodynamic origin is expected here, since it is at the end of the potential core. The relevance of these fluctuations is currently a subject of active debate [47,48].

The total amplification experienced by the wavepackets is quantified using the N-factor, defined as

$$N = \log\left(\left|\frac{A(x)}{A(x_0)}\right|\right) = -\int_{x_0}^{x} \alpha_i(\xi)\,\mathrm{d}\xi \tag{14}$$

(cf. Eq. (2)), for Strouhal numbers $St = 0.3$ and $S = 0.5$ and different spacings of the jets spanning from $h = 1.1\,D$ to $1.8\,D$. The results are shown in Fig. 11. Fig. 12 shows the corresponding wavepacket amplitudes, illustrating the amplitude growth and phase speed variations along the axial direction simultaneously. In line with the fluctuation fields visualizations discussed above, a weak destabilizing due to jet proximity is found on $m = 0$ S wavepackets, which is slightly more pronounced for the lower $St = 0.3$ frequency. Conversely, a dramatic impact of the jet separation on the amplitude growth is observed for $m = 0$ A, which varies from a strong stabilization for lower frequencies and jet separations to an important destabilization for relatively higher frequencies and bounded ranges of jet distances. For instance, Fig. 12 (bottom right) shows, for $St = 0.5$ and modes $m = 0S$, a maximum amplification of $A(x)/A(x_0) \approx 93.2$ ($N \approx 4.5$) for $h = 1.5D$; for $h = 1.3D$ the corresponding amplification is $A(x)/A(x_0) \approx 34.6$ ($N \approx 3.5$), occurring around two diameters closer to the nozzle lips. On the other hand, $A(x)/A(x_0) \approx 1.89$ ($N \approx 0.6$) for $h = 1.1D$.

4. Conclusions

With the objective of modeling the large-scale turbulent structures present in the turbulent mixing region of twin-jet configurations, the standard PSE methodology is extended to consider wave-like instabilities with an arbitrary dependence of their properties in the cross-stream plane. This methodology, relatively recent in the literature, is herein referred to as three-dimensional PSE or 3D PSE, as opposed to the usual PSE applications in which the spanwise or azimuthal directions are introduced using Fourier modes. For its initialization, a locally-parallel spatial instability analysis is performed.

The $M_j = 0.4$ single round jet from previous publications [14,28] is used to construct mean flow models for twin-jet configurations, by the combination of the velocity fields for two ideal jets. The resulting flows agree qualitatively with the experimental observations by Okamoto et al. [45], but quantitative agreement with real twin-jet mean flows is expected only for the first few diameters of evolution, in the jets' pre-merging region. Future research in this direction should consider more realistic mean flows, obtained from experiments or high-fidelity simulations. Previous experiences on the computation of wavepackets using PSE for single round jets demonstrated that small inaccuracies in the mean flow gradients can result in important differences in the PSE solutions.

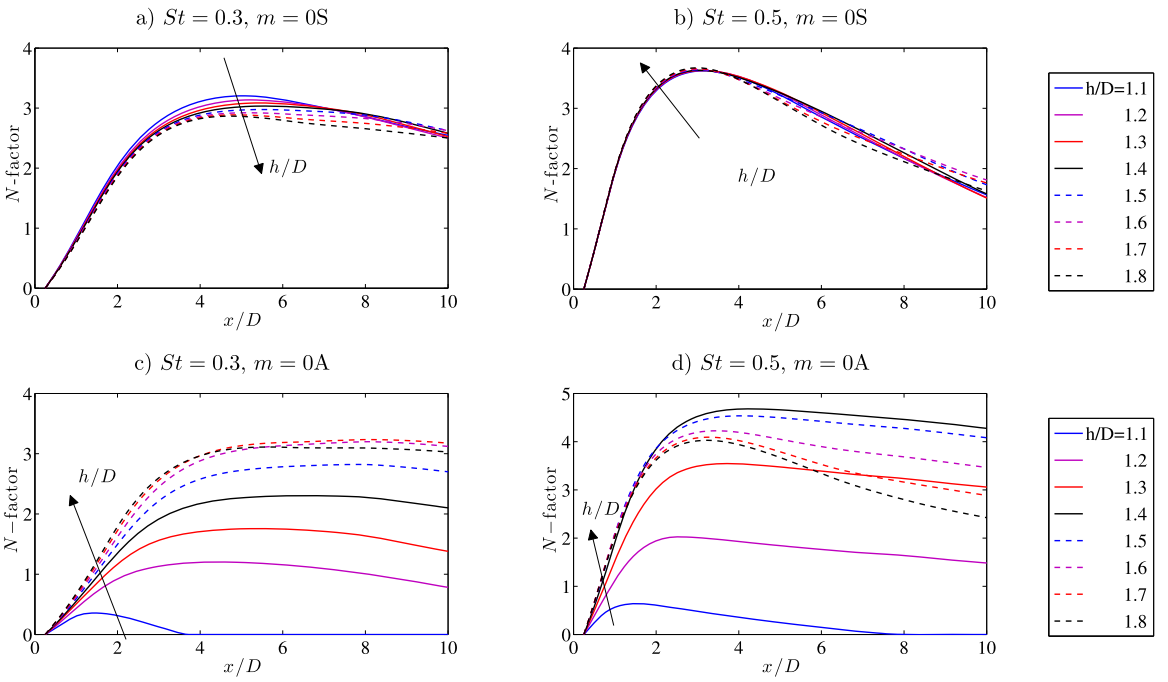

Fig. 11. Amplification curves, in terms of the N-factor corresponding to $St = 0.3$ and $St = 0.5$ and modes $m = 0$ S, and $m = 0$ A, for jet separations $h/D = 1.1, 1.2, 1.3, 1.4, 1.5, 1.6, 1.7$, and 1.8, increasing in the direction of the arrows.

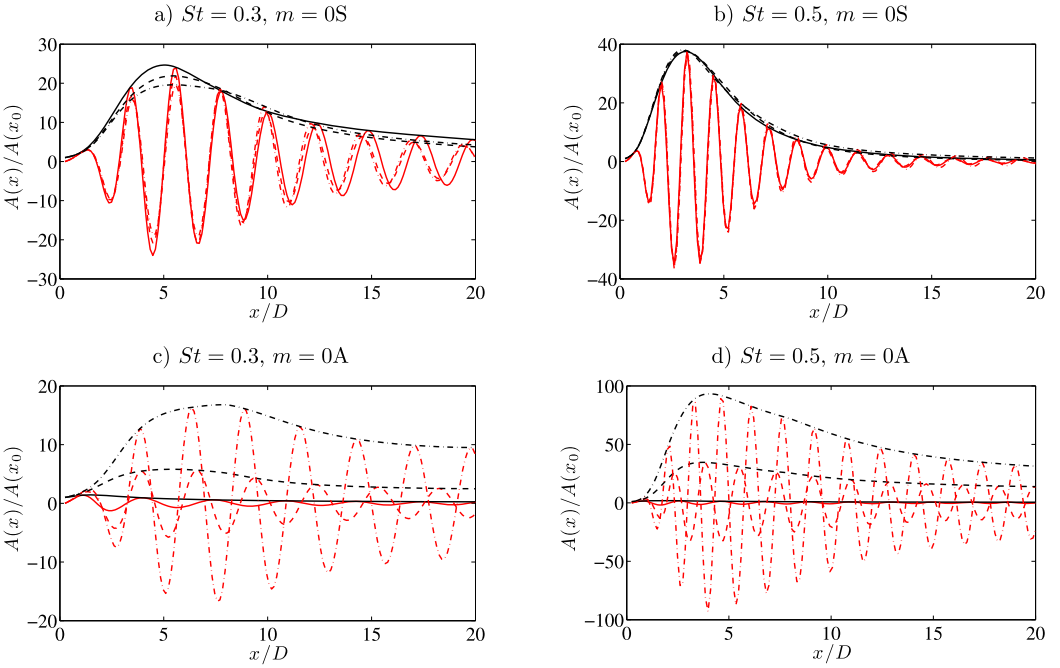

Fig. 12. Real component of the amplitude curves $A(x)$, corresponding $St = 0.3$ and $St = 0.5$ and modes $m = 0$ S, and $m = 0$ A, for jet separations $h/D = 1.1$ (solid lines), 1.3 (dashed lines), and 1.5 (dashed-dotted lines).

Local stability analyses presented herein for near-nozzle cross-planes show that the jet interaction has the potential to stabilize and destabilize the Kelvin–Helmholtz instabilities. The effects of jet proximity are stronger for lower frequencies and azimuthal wavenumbers. Particular attention is paid to two eigenmodes, corresponding to the axisymmetric mode ($m = 0$) for single jets. The $m = 0$ mode has been suggested to be the most relevant one for the noise radiated by single jets [14], partly due to the more elongated structure of the corresponding wavepacket, higher peak amplitudes, and slower radial decay of their associated pressure field, as compared to $|m| \geq 1$ azimuthal modes. For twin jets, the azimuthal symmetry

of this mode is broken, and two discrete modes appear: a faster one ($m = 0$ A), which is antisymmetric about the jet mid-plane and is related to sinuous fluctuations of the flow field, and a slower and symmetric one ($m = 0$ S) related to varicose fluctuations. Inspection of their respective pressure fields shows that $m = 0$ S retains the asymptotic behavior of the axisymmetric mode, but $m = 0$ A behaves asymptotically as a $m = 1$ mode. Wavepackets arising from the $m = 0$ A modes near the nozzle can be expected to be significantly less efficient in generating sound.

The results presented herein show that jet proximity has a limited effect on $m = 0$ S modes, exerting a mild destabilization when their separation is reduced. The amplitude peak of the pressure fluctuations is localized in the external shear layer of the twin-jet mean flow. Conversely, the jet separation has a dramatic effect on the spatial growth and subsequent decay of the $m = 0$ A modes. Order-of-magnitude changes in the wavepacket amplification are found for different combinations of the jet separation and Strouhal number, ranging from strong stabilizations for low frequencies and very close jets, to significant destabilization for particular frequency ranges and jet separations $h \sim 1.5\,D$. Maximum amplitudes found for $m = 0$ A wavepackets clearly exceed those for $m = 0$ S. Furthermore, the maxima of the pressure and velocity fluctuations are localized in the merging region between the two jets for the asymmetric modes.

The full implications of present wavepacket models for twin-jet configurations with noise radiation are unclear at present, as is the relation between wavepacket models for single round jets and the far-field sound [47–49]. Some experiments [23,24] have reported the presence of sinuous oscillations of the twin-jet flow field associated with net reductions of the far-field sound pressure levels and changes in the sound directionality on the azimuthal direction, for certain combinations of parameters. This behavior can be attributed to the dominance of the $m = 0$ A mode described here. It may therefore be conjectured that noise reductions in twin-jet configurations may be achieved by favoring the appearance of this instability in a controlled manner.

Acknowledgements

The authors are indebted to Peter Jordan and Lutz Lesshafft for suggesting the use of the tailored mean flow for the twin-jet configuration, and to one of the anonymous referees for suggesting the introduction of the first appendix. D.R. thanks L. Lesshafft, P. Jordan, and A. Awargal for the invitation to present this work at the Euromech Colloquium 571 – IUTAM Symposium on Jet Noise Modelling and Control, École polytechnique, Palaiseau, France, September 28–30, 2016. The authors also acknowledge funding from the Brazilian National Council for Scientific and Technological Development CNPq (grants 405144/2016-4, 305512/2016-1, 150500/2016-5, 423846/2016-7), São Paulo Research Foundation FAPESP (grants 2014/24782-0, 2017/01586-0) and Rio de Janeiro Research Foundation FAPERJ (grant 233386).

Appendix A. On the use of PSE for computing wavepackets

The use of PSE for the computation of large-scale structures in turbulent flows deserves some additional comments. The parabolized stability equations were originally devised as an outgrowth of the weakly non-parallel analysis for the study of instability and transition of laminar flow. The exponential form of the Ansatz – Eq. (2) – assumes that a single relevant *local* eigenmode exists, characterized by its wavenumber and spatial structure. The downstream integration tries to follow this eigenmode, accounting for the downstream history of the disturbance and slow divergence of the base flow. The results of PSE are in general robust, and their interpretation is straightforward in those cases in which a single, unstable local eigenmode exists for each frequency, as is the case of laminar flat-plate boundary layers [29–31]. When an unforced turbulent jet flow is considered, some problems are encountered.

For isolated round jets, comparisons between PSE computations and wavepacket structures educed from experimental data using the Proper Orthogonal Decomposition show very good agreement in the near-field pressure and velocity fields for the first diameters downstream of the nozzle, up to the end of the potential core [13,14]. Rodríguez et al. [17] used a bi-orthogonal projection of large eddy simulation data on the different local eigenmode families to conduct PSE computations with different initial conditions. It was found that, as far as the contribution of the single unstable Kelvin–Helmholtz eigenmode was introduced in the initial fluctuation shape function, PSE converges quickly to the same solution regardless of contributions from other (stable) eigenmodes. When the initial condition did not include the Kelvin–Helmholtz eigenmode, the result of the integration was not robust. This behavior was further investigated by monitoring simultaneously the downstream evolution of the locally-parallel stability eigenspectra and the PSE solution [28]. Wavepacket models computed by PSE are robust and compare well with experiments when a single unstable eigenmode exist. As the integration advances towards the end of the potential core, the discrete Kelvin–Helmholtz eigenmode first becomes stable and finally merges with the continuous branch of vorticity modes; in the absence of a dominant eigenmode, the PSE solution captures a partial and limited combination of eigenmodes, with axial wavelengths close to that followed by the PSE integration.

These observations explain the good agreement of PSE computations with the dominant turbulent coherent structures extracted from experiments [13,14,28], high-fidelity simulations [17,18] and the leading mode of global resolvent analysis [21,50] for spatial regions in which a dominant, physical instability mechanism exists, with which the discrete unstable eigenmode is associated. Once a dominant modal instability is absent, the dynamics become too complex for the PSE to capture. Alternative methodologies, either based on two-dimensional eigenmode problems [19,20], global resolvent analysis [21,50], or the one-way linearized equations [22] are promising in the modeling of the dynamics of the aft part of the wavepackets.

The PSE computations face additional difficulties when multiple unstable discrete modes exist, as the integration tends to follow the most unstable one. In the present work, several unstable modes coexist, resulting from the coupled discretization of the two-dimensional plane and the interaction between the two jets. Local eigenmodes related to $|m| = 2, 3$ and 4 (depending on St) are the most unstable ones at the nozzle lip, but are damped a short distance downstream. Modes corresponding to $m = 0$ are the most relevant ones for noise generation, and become the most unstable ones as the $|m| \geq 2$ decay. Special care had to be taken to prevent the PSE solutions from "shifting" from one mode to another. The tendency to this shifting is increased by the proximity of the wavenumber α, the similarity of the shape function $\tilde{\mathbf{q}}$, and the step size Δx. The strategy adopted here was the reduction of the step size so that important variations of α and $\tilde{\mathbf{q}}$ cannot appear between two consecutive steps. The stabilization procedure (8) and careful choice of the parameters (9) was instrumental in delivering robust solutions.

Appendix B. Governing equations

The set of equations used as the departure point in the derivation of the locally-parallel stability analysis and the parabolized stability equations, corresponding to the non-conservative version of those used by [51], is listed below:

$$\frac{\partial \rho}{\partial t} + \frac{\partial (\rho u_j)}{\partial x_j} = 0 \tag{15}$$

$$\rho \left(\frac{\partial u_i}{\partial t} + u_j \frac{\partial u_i}{\partial x_j} \right) + \frac{\partial p}{\partial x_i} - \frac{\partial \tau_{ij}}{\partial x_j} = 0 \tag{16}$$

$$\rho \left(\frac{\partial e}{\partial t} + u_j \frac{\partial e}{\partial x_j} \right) + \frac{\partial p u_j}{\partial x_j} + \frac{\partial (-\tau_{ik} u_i + q_j)}{\partial x_j} = 0 \tag{17}$$

where $(x_1, x_2, x_3) = (x, y, z)$ are the Cartesian coordinates, $(u_1, u_2, u_3) = (u, v, w)$ the corresponding velocity components, and the specific energy e, the viscous stress tensor τ_{ij} and the heat flux for a fluid obeying Fourier's law, q_j, are given by

$$e = \frac{1}{\gamma - 1} \frac{p}{\rho} + \frac{1}{2} u_i u_i \tag{18}$$

$$\tau_{ij} = \frac{\mu}{Re} \left(\frac{\partial u_i}{\partial x_j} + \frac{\partial u_j}{\partial x_i} - \frac{2}{3} \frac{\partial u_k}{\partial x_k} \right) \tag{19}$$

and

$$q_j = -\frac{\mu}{Re\, Pr} \frac{\partial T}{\partial x_i} \tag{20}$$

Here γ is the ratio of specific heats, μ is the viscosity coefficient, Re is the Reynolds number and Pr is the Prandtl number. The set of equations is closed by the equation of state

$$p = \frac{\gamma - 1}{\gamma} \rho T \tag{21}$$

While linearizing the equations, density $\bar{\rho}$, and temperature $\bar{T}$ are retained for the base flow description, while the perturbations are written down in terms of pressure p' and temperature T'. The equation of state (21) particularized for the based flow is substituted in the governing equations, while the linear perturbation density term takes the form

$$\rho' = \frac{\gamma}{\gamma - 1} \frac{p'}{\bar{T}} - \frac{\bar{\rho}}{\bar{T}} T' \tag{22}$$

The linear operators $\mathbf{L}$ and $\mathbf{R}$ are obtained by substituting the PSE Ansatz (2) in the linearized governing equations and by neglecting second-order streamwise derivatives of the base flow quantities. These derivations were done using the symbolic computing software *Maple*, and validated by reproducing the results of [14,28].

References

[1] E. Mollo-Christensen, Jet noise and shear flow instability seen from an experimenter's viewpoint, J. Appl. Mech. 34 (1967) 1–7.
[2] P. Jordan, T. Colonius, Wave packets and turbulent jet noise, Annu. Rev. Fluid Mech. 45 (1) (2013) 173–195.
[3] D.G. Crighton, P. Huerre, Shear-layer pressure fluctuations and superdirective acoustic sources, J. Fluid Mech. 220 (1990) 355–368.
[4] C.K.W. Tam, Supersonic jet noise, Annu. Rev. Fluid Mech. 27 (1) (1995) 17–43.
[5] A.V.G. Cavalieri, P. Jordan, T. Colonius, Y. Gervais, Axisymmetric superdirectivity in subsonic jets, J. Fluid Mech. 704 (2012) 388–420.
[6] D. Juvé, M. Sunyach, G. Compte-Bellot, Intermittency in the noise emission in subsonic cold jets, J. Sound Vib. 71 (1980) 319–332.
[7] J.I. Hileman, B.S. Thurow, E.J. Caraballo, M. Samimy, Large-scale structure evolution and sound emission in high-speeds jets: real-time visualization with simultaneous acoustic measurements, J. Fluid Mech. 544 (2005) 277–307.
[8] A.V.G. Cavalieri, G. Daviller, P. Comte, P. Jordan, G. Tadmor, Y. Gervais, Using large eddy simulation to explore sound-source mechanisms in jets, J. Sound Vib. (330) (2011) 4098–4113.

[9] S. Crow, F. Champagne, Orderly structure in jet turbulence, J. Fluid Mech. 48 (3) (1971) 547–591.
[10] D.G. Crighton, M. Gaster, Stability of slowly diverging jet flow, J. Fluid Mech. 77 (2) (1976) 397–413.
[11] A. Michalke, Survey on jet instability theory, Prog. Aerosp. Sci. 21 (1984) 159–199.
[12] T. Suzuki, T. Colonius, Instability waves in a subsonic round jet detected using a near-field phased microphone array, J. Fluid Mech. 565 (2006) 197–226.
[13] K. Gudmundsson, T. Colonius, Instability wave models for the near-field fluctuations of turbulent jets, J. Fluid Mech. 689 (2011) 97–128.
[14] A.V.G. Cavalieri, D. Rodríguez, P. Jordan, T. Colonius, Y. Gervais, Wavepackets in the velocity field of turbulent jets, J. Fluid Mech. 730 (2013) 559–592.
[15] E. Piot, G. Casalis, F. Muller, C. Bailly, Investigation of the PSE approach for subsonic and supersonic hot jets. Detailed comparisons with LES and linearized Euler equations results, Int. J. Aeroacoust. 5 (2006) 361–393.
[16] P.K. Ray, L.C. Cheung, S.K. Lele, On the growth and propagation of linear instability waves in compressible turbulent jets, Phys. Fluids 21 (2009) 054106.
[17] D. Rodríguez, A. Sinha, G. Brès, T. Colonius, Inlet conditions for wave packet models in turbulent jets based on eigenmode decomposition of large eddy simulation data, Phys. Fluids 25 (2013) 105107.
[18] A. Sinha, D. Rodríguez, G. Brès, T. Colonius, Wavepacket models for supersonic jet noise, J. Fluid Mech. 742 (2014) 71–95.
[19] J.W. Nichols, S.K. Lele, Global modes and transient response of a cold supersonic jet, J. Fluid Mech. 669 (2011) 225–241.
[20] X. Garnaud, L. Lesshafft, P.J. Schmid, P. Huerre, Modal and transient dynamics of jet flows, Phys. Fluids 25 (2013) 044103.
[21] X. Garnaud, L. Lesshafft, P.J. Schmid, P. Huerre, The preferred mode of incompressible jets: linear frequency response analysis, J. Fluid Mech. 716 (2013) 189–202.
[22] A. Towne, T. Colonius, One-way spatial integration of hyperbolic equations, J. Comput. Phys. 300 (2015) 844–861.
[23] W.V. Bhat, Acoustic Characteristics of Two Parallel Flow Jets, AIAA Paper 77-1290, 1977.
[24] R.A. Kantola, Acoustic properties of heated twin jets, J. Sound Vib. 79 (1) (1981) 79–106.
[25] P.J. Morris, Instability waves in twin supersonic jets, J. Fluid Mech. 220 (1990) 293–307.
[26] M.R. Green, D.G. Crighton, Instability properties of interacting jets, J. Fluid Mech. 350 (1997) 331–349.
[27] M. Broadhurst, S. Sherwin, The parabolised stability equations for 3D-flows: implementation and numerical stability, Appl. Numer. Math. 58 (7) (2008) 1017–1029.
[28] D. Rodríguez, A.V.G. Cavalieri, T. Colonius, P. Jordan, A study of linear wavepacket models for subsonic turbulent jets using local eigenmode decomposition of PIV data, Eur. J. Mech. B, Fluids 49 (2015) 308–321.
[29] F.P. Bertolotti, Th. Herbert, P.R. Spalart, Linear and nonlinear stability of the Blasius boundary layer, J. Fluid Mech. 242 (1992) 441–474.
[30] C-L. Chang, M.R. Malik, G. Erlenbacher, M.Y. Hussaini, Linear and Nonlinear PSE for Compressible Boundary Layers, ICASE Report No. 93-70, 1993.
[31] T. Herbert, Parabolized stability equations, Annu. Rev. Fluid Mech. 29 (1997) 245–283.
[32] L.M. Mack, Boundary layer linear stability theory, AGARD-R-709 Special course on stability and transition of laminar flow, 1984, 3.1–3.81.
[33] P. Balakumar, M.R. Malik, Discrete modes and continuous spectra in supersonic boundary layer, J. Fluid Mech. 239 (1992) 631–656.
[34] D. Rodríguez, V. Theofilis, Massively parallel numerical solution of the biglobal linear instability eigenvalue problem using dense linear algebra, AIAA J. 47 (10) (2009) 2449–2459.
[35] V. Theofilis, Global linear stability, Annu. Rev. Fluid Mech. 43 (2011) 319–352.
[36] E.M. Gennaro, D. Rodríguez, M.A.F. Medeiros, V. Theofilis, Sparse techniques in global flow instability with application to compressible leading-edge flow, AIAA J. 51 (9) (2013) 2295–2303.
[37] D. Rodríguez, E.M. Gennaro, Three-dimensional flow stability analysis based on the matrix-forming approach made affordable, in: J.S. Hesthaven (Ed.), Spectral and High Order Methods for Partial Differential Equations ICOSAHOM 2016, in: Lect. Notes Comput. Sci. Eng., vol. 199, Springer, 2017.
[38] W.E. Arnoldi, The principle of minimized iterations in the solution of the matrix eigenvalue problem, Q. Appl. Math. 9 (1951) 17–29.
[39] G.H. Golub, C.F. Van Loan, Matrix Computations, Johns Hopkins University Press, 1996.
[40] P.R. Amestoy, I.S. Duff, J.-Y. L'Excellent, J. Koster, A fully asynchronous multifrontal solver using distributed dynamic scheduling, SIAM J. Matrix Anal. Appl. 23 (1) (2001) 15–41.
[41] F. Li, M.R. Malik, Spectral analysis of parabolized stability equations, Comput. Fluids 26 (3) (1997) 279–297.
[42] P. Andersson, D.S. Henningson, A. Hanifi, On a stabilization procedure for the parabolic stability equations, J. Eng. Math. 33 (1998) 311–332.
[43] T.R. Troutt, D.K. McLaughlin, Experiments on the flow and acoustic properties of a moderate Reynolds number supersonic jet, J. Fluid Mech. 116 (1982) 123–156.
[44] C.K.W. Tam, D.E. Burton, Sound generated by instability waves of supersonic flows. Part 2. Axisymmetric jets, J. Fluid Mech. 138 (1984) 273–295.
[45] T. Okamoto, M. Yagita, A. Watanabe, K. Kawamura, Interaction of twin turbulent circular jets, Bull. JSME 28 (238) (1985) 617–622.
[46] A.E. Gill, Instabilities of Top-Hat jets and wakes in compressible fluids, Phys. Fluids 8 (1965) 1428–1430.
[47] A. Towne, T. Colonius, P. Jordan, A.V.G. Cavalieri, G. Brès, Stochastic and nonlinear forcing of wavepackets in a Mach 0.9 jet, in: 21st AIAA/CEAS Aeroacoustics Conference, AIAA, Dallas, TX, 2015.
[48] O. Semeraro, V. Jaunet, P. Jordan, A.V.G. Cavalieri, L. Lesshafft, Stochastic and harmonic optimal forcing in subsonic jets, in: 22nd AIAA/CEAS Aeroacoustics Conference, AIAA, Lyon, France, 2016.
[49] D.E.S. Breakey, P. Jordan, A.V.G. Cavalieri, P.A. Nogueira, O. Léon, T. Colonius, D. Rodríguez, Experimental study of turbulent-jet wave packets and their acoustic efficiency, Phys. Rev. Fluids 2 (2017) 124601.
[50] S. Beneddine, D. Sipp, A. Arnault, J. Dandois, L. Lesshafft, Conditions for validity of mean flow stability analysis, J. Fluid Mech. 798 (2016) 485–504.
[51] W.R. Wolf, J.L.F. Azevedo, S.K. Lele, Convective effects and the role of quadrupole sources for aerofoil aeroacoustics, J. Fluid Mech. 708 (2012) 502–538.